Journal for ImmunoTherapy of Cancer

Therapeutic efficacy of antibody-drug conjugates targeting GD2-positive tumors

Daniel V Kalinovsky ,[1] Alexey V Kibardin,[2] Irina V Kholodenko,[3] Elena V Svirshchevskaya,[1] Igor I Doronin,[1,4] Mariya V Konovalova ,[1] Maria V Grechikhina,[1] Fedor N Rozov,[5] Sergey S Larin,[2] Sergey M Deyev,[1,6] Roman V Kholodenko [1,4]

To cite: Kalinovsky DV, Kibardin AV, Kholodenko IV, *et al*. Therapeutic efficacy of antibody-drug conjugates targeting GD2-positive tumors. *Journal for ImmunoTherapy of Cancer* 2022;**10**:e004646. doi:10.1136/jitc-2022-004646

► Additional supplemental material is published online only. To view, please visit the journal online (http://dx.doi.org/10.1136/jitc-2022-004646).

Accepted 01 June 2022

[1]Department of Immunology, Shemyakin-Ovchinnikov Institute of Bioorganic Chemistry, Russian Academy of Sciences, Moscow, Russia
[2]Dmitriy Rogachev National Medical Research Center of Pediatric Hematology, Oncology, and Immunology, Moscow, Russia
[3]Orekhovich Institute of Biomedical Chemistry, Moscow, Russia
[4]Real Target LLC, Moscow, Russia
[5]Lomonosov Moscow State University, Moscow, Russia
[6]Sechenov First Moscow State Medical University, Moscow, Russia

Correspondence to
Dr Roman V Kholodenko; khol@mail.ru

ABSTRACT

Background Both ganglioside GD2-targeted immunotherapy and antibody-drug conjugates (ADCs) have demonstrated clinical success as solid tumor therapies in recent years, yet no research has been carried out to develop anti-GD2 ADCs against solid tumors. This is the first study to analyze cytotoxic activity of clinically relevant anti-GD2 ADCs in a wide panel of cell lines with varying GD2 expression and their effects in mouse models of GD2-positive solid cancer.

Methods Anti-GD2 ADCs were generated based on the GD2-specific antibody ch14.18 approved for the treatment of neuroblastoma and commonly used drugs monomethyl auristatin E (MMAE) or F (MMAF), conjugated via a cleavable linker by thiol-maleimide chemistry. The antibody was produced in a mammalian expression system, and its specific binding to GD2 was analyzed. Antigen-binding properties and biodistribution of the ADCs in mice were studied in comparison with the parent antibody. Cytotoxic effects of the ADCs were evaluated in a wide panel of GD2-positive and GD2-negative tumor cell lines of neuroblastoma, glioma, sarcoma, melanoma, and breast cancer. Their antitumor effects were studied in the B78-D14 melanoma and EL-4 lymphoma syngeneic mouse models.

Results The ch14.18-MMAE and ch14.18-MMAF ADCs retained antigen-binding properties of the parent antibody. Direct dependence of the cytotoxic effect on the level of GD2 expression was observed in cell lines of different origin for both ADCs, with IC50 below 1 nM for the cells with high GD2 expression and no cytotoxic effect for GD2-negative cells. Within the analyzed cell lines, ch14.18-MMAF was more effective in the cells overexpressing GD2, while ch14.18-MMAE had more prominent activity in the cells expressing low GD2 levels. The ADCs had a similar biodistribution profile in the B78-D14 melanoma model compared with the parent antibody, reaching 7.7% ID/g in the tumor at 48 hours postinjection. The average tumor size in groups treated with ch14.18-MMAE or ch14.18-MMAF was 2.6 times and 3.8 times smaller, respectively, compared with the control group. Antitumor effects of the anti-GD2 ADCs were also confirmed in the EL-4 lymphoma model.

Conclusion These findings validate the potential of ADCs targeting ganglioside GD2 in treating multiple GD2-expressing solid tumors.

WHAT IS ALREADY KNOWN ON THIS TOPIC

⇒ Despite significant progress in the development of GD2-targeted immunotherapy and strong potential of antibody-drug conjugates (ADCs) realized in more than 10 approved drugs, no studies have addressed anti-GD2 ADCs in recent years.

WHAT THIS STUDY ADDS

⇒ Anti-GD2 antibodies conjugated to the microtubule-depolymerizing agents monomethyl auristatin E or F were generated that maintained stability, antigen-binding properties, and the in vivo biodistribution profile of the parent antibody.
⇒ The ADCs demonstrated potent and highly selective cytotoxicity in vitro in a number of tumor cell lines of neuroblastoma, glioma, breast cancer, sarcoma, and melanoma.
⇒ Strong inhibition of tumor growth was observed for the ADCs in syngeneic mouse models of B78-D14 melanoma and EL-4 lymphoma.

HOW THIS STUDY MIGHT AFFECT RESEARCH, PRACTICE, OR POLICY

⇒ The results of the study suggest the applicability of anti-GD2 ADCs for treating a broad spectrum of GD2-expressing tumors.

INTRODUCTION

Cancer immunotherapy with antibody-drug conjugates (ADCs) is a potent strategy that has gained strong evidence of efficacy in recent years. To date 11 antibodies conjugated with small molecule drugs were approved by the US Food and Drug Administration for oncology indications, 7 of which in the past 3 years, and at least 80 more ADCs are under development in 150 active clinical trials.[1 2] While the currently approved drugs are indicated for the treatment of both hematologic (6 ADCs) and solid malignancies (5 ADCs), over 80% of ADCs in active clinical trials are being investigated for solid tumor therapy.[1 3] Immunotherapeutics often have

reduced efficacy in solid tumors compared with hematologic malignancies,[4] but the increase in the number of ADCs in clinical trials for solid tumors may suggest their high therapeutic potential to overcome problems as antigen heterogeneity or physical barriers in the tumor microenvironment.

Three of the five ADCs approved for solid tumors target breast cancer. Trastuzumab emtansine (T-DM1) shows significant efficacy and safety benefit as second-line treatment of HER2-positive breast cancer compared with a combination of trastuzumab and chemotherapy.[5] Newer generation trastuzumab deruxtecan demonstrates improved potency versus T-DM1 due to a cleavable linker and a higher number of exatecan derivative molecules that exert bystander cell killing in heterogeneous tumors with varying levels of HER2 expression.[6] Approval of sacituzumab govitecan that targets a different marker Trop-2 in triple-negative breast cancer (TNBC)[3] further emphasizes the importance of ADCs in breast cancer therapy. The two ADCs approved for solid tumors aside from breast cancer are enfortumab vedotin indicated for nectin-4 positive urothelial cancer and tisotumab vedotin indicated for tissue factor-expressing cervical cancer, both carrying the monomethyl auristatin E (MMAE) drug via the protease-cleavable valine-citrulline linker.[1]

Ganglioside GD2 is an established target in cancer immunotherapy that is overexpressed in neuroblastoma, glioma, melanoma, various sarcomas, small cell lung cancer, breast cancer, and a number of other tumors.[7 8] Structurally, GD2 represents a glycosphingolipid composed of a ceramide and two sialic acid residues linked to three monosaccharide units. Only two drugs, dinutuximab and naxitamab, GD2-specific monoclonal antibodies of the 14.18/14G2a and 3F8 families, respectively, have been approved for targeted therapy of GD2-positive tumors. They are used in combination therapy of high-risk neuroblastoma and significantly increase patient survival.[9 10] Additionally, various alternative GD2-directed strategies are explored that primarily address the insufficient efficacy of naked full-length antibodies in eliminating GD2-positive tumors—therapies based on adoptive chimeric antigen receptor (CAR) T or NK cells, bispecific antibodies, immunocytokines, vaccines, radioimmunopharmaceuticals, and immunotoxins.[11 12]

Despite their apparent therapeutic potential, very limited research has been carried out on ADCs targeting GD2-positive tumors. If ADCs are classified as antibody conjugates with small-molecule drugs and not biological toxins, then only one article regarding anti-GD2 ADCs dated 1998 is present in open literature.[13] This important early work describes the generation of a conjugate based on the GD2-specific antibody 14G2a thiol conjugated to a calicheamicin analog. The resulting conjugate was shown to significantly suppress liver metastases in a mouse model of neuroblastoma, however the metastasis model used in the work leaves questions about the effectiveness of anti-GD2 ADCs in eliminating solid tumor growth. Also, the described ADC is currently not optimal both in terms of the choice of the drug and its conjugation to the antibody.

The objective of our work was to develop clinically relevant anti-GD2 ADCs and assess their efficacy in eliminating GD2-positive solid tumors in order to determine the applicability of GD2 as a target for ADCs. For this, we generated ADCs based on the GD2-specific chimeric antibody 14.18 approved for neuroblastoma treatment and the microtubule-depolymerizing agents MMAE or MMAF linked to the antibody interchain disulfides by the commonly used valine-citrulline linker. Antigen-binding properties of the conjugates and their biodistribution in mice were analyzed in comparison with the parent antibody. For the first time, cytotoxic effects of anti-GD2 ADCs were evaluated in a wide panel of GD2-positive and GD2-negative tumor cell lines. Antitumor effects of the ADCs were investigated in GD2-positive solid syngeneic mouse models of B78-D14 melanoma and EL-4 lymphoma.

MATERIALS AND METHODS

ADC generation

The ch14.18 antibody was conjugated to MC-VC-PABC-MMAE or MC-VC-PABC-MMAF (both from BOC Sciences), further referred to as MMAE or MMAF. Partial reduction of cysteines forming disulfide bonds between antibody chains was performed using 1 mM tris (2-carboxyethyl)phosphine (TCEP) in 50 mM potassium phosphate—5 mM EDTA solution at pH 6.0, for 1 hour at 37°C and with gentle agitation. The reducing agent was then removed by a Zeba Spin Desalting Column, 7K MWCO (Thermo Fisher Scientific), followed by an immediate reaction of 3 mg/mL antibody with 7:1 molar excess of the drug (for conjugates with optimized drug-to-antibody ratio (DAR) 4) for 3 hours at 37°C. Alternatively, simultaneous cysteine reduction and conjugation with maleimide-activated MMAE or MMAF was performed by incubating the antibody with 1 mM TCEP and 7:1 excess of drug for 3 hours, yielding a product with lower DAR. ADCs were transferred to phosphate-buffered saline (PBS) in Zeba columns. The antibody was also conjugated to 6-maleimidocaproyl hydrazone derivative of doxorubicin (DOX, MedChemExpress) and fluorescein 6-maleimide (FAM-maleimide, Lumiprobe) in reaction conditions identical to those described above. Products were purified by size-exclusion chromatography on a Superdex 200 10/300 GL column (GE Healthcare). Average DAR for antibody conjugates with MMAE or MMAF, as well as degree of labeling (DOL) for conjugates with aldoxorubicin or FAM-maleimide were calculated by ultraviolet-visible (UV-VIS) spectroscopy on a BioDrop µLITE spectrophotometer (Biochrom), as described by Chen.[14] Coefficients for calculating the DAR for ch14.18-MMAE and ch14.18-MMAF are presented in online supplemental table S1. Visualization of the ADCs and the ch14.18 antibody was performed by reducing SDS-polyacrylamide gel electrophoresis (PAGE), as described before.[15]

Direct ELISA

Nunc MaxiSorp high protein-binding capacity 96 well ELISA plates (Thermo Fisher Scientific) were coated with gangliosides GD2, GM2, GD1b, and GD3 at concentration of 0.25 µg in 100 µl of 96% ethanol per well. GD2, GD1b, and GD3 were purchased from Sigma-Aldrich, and GM2 was obtained according to our previous work.[16] The detailed procedure is described in online supplemental file 1.

Cell lines

GD2-positive B78-D14 mouse melanoma cell line was derived from GD2-negative B16 cells by transfection with genes coding for GD3 and GD2 synthases, as described by Haraguchi *et al*.[17] B78-D14 melanoma was cultured in RPMI-1640 medium supplemented with 10% fetal bovine serum (FBS), 2 mM L-glutamine, 1 mM sodium pyruvate, 1× non-essential amino acids solution (all from Gibco), 400 µg/mL G418, and 500 µg/mL hygromycin B (both from Sigma-Aldrich).

EL-4 mouse lymphoma was cultured in RPMI-1640 medium, IMR-32 human neuroblastoma – in EMEM medium. NGP-127 and SH-SY5Y human neuroblastomas, T98G, 1321N1, and U87MG human gliomas, U2OS, MG-63, and HOS human osteosarcomas, Hs578T, MCF-7, and SKBr3 human breast cancer lines, COLO-38, mS, and A375 human melanomas, and B16 and M3 mouse melanomas were cultured in DMEM medium. All media were supplemented with 10% heat-inactivated FBS, 2 mM *L*-glutamine, 100 µg/mL penicillin, and 100 U/mL of streptomycin (all from Gibco).

IMR-32, SH-SY5Y, T98G, U87MG, Hs578T, MCF-7, U2OS, MG-63, A375, HOS, and EL-4 cell lines were obtained from the American Type Culture Collection; NGP-127, 1321N1, mS, B16, and M3 cell lines were kindly provided by Anton Buzdin (Shemyakin-Ovchinnikov Institute of Bioorganic Chemistry RAS, Russia). The B78-D14 cell line was a kind gift from David Schrama (University Hospital Wuerzburg, Germany). All cell lines were maintained at low passage numbers and routinely checked for mycoplasma by PCR. Authentication by STR analysis was performed for human cell lines.

Flow cytometry

Staining of the cells with ch14.18-FAM was performed as described previously.[18] Cells were detached from culture plates (adherent cells were trypsinized and washed twice in PBS), incubated with ch14.18-FAM or 14G2a-AF488 (Santa Cruz Biotechnology) (1 µg per 10^6 cells) for 1 hour in PBS supplemented with 1% FBS and 0.02% sodium azide, and washed twice in PBS. All procedures were performed at 4°C. The samples were immediately analyzed using EPICS Coulter XL-MCL flow cytometer (Beckman Coulter). At least 5000 events were collected in each sample. For all samples, the analysis was performed in triplicate. Data were analyzed using WinMDI V.2.8 software.

MTT assay

ADC-induced decrease in cell viability was analyzed by colorimetric MTT (3-(4,5-dimethylthiazol-2-yl)−2,5-diphenyltetrazolium bromide, Sigma-Aldrich) assay, as described earlier.[19] See online supplemental file 1 for details.

Biodistribution studies

For generation of fluorescently labeled ch14.18-MMAE with low DAR and its parent antibody, the molecules were conjugated with the fluorescent dye Sulfo-Cyanine5 NHS ester (Sulfo-Cy5-NHS, Lumiprobe) via side chain amine groups of lysine. The dye was added to the ADC or naked antibody in 0.1 M bicarbonate buffer, pH 8.3, in a molar excess of 5:1, followed by incubation for 3 hours in the dark at room temperature with gentle agitation. The product was purified from unreacted dye in a Zeba column. DOL was calculated by UV-VIS spectroscopy as described before[14] and was highly consistent for different batches of the labeled ch14.18-MMAE and its parent antibody in the range of 1.9–2.

Female 6–8 weeks old C57BL/6 mice were obtained from Shemyakin-Ovchinnikov Institute of Bioorganic Chemistry RAS and kept in a clean barrier facility in microisolator cages.

Subcutaneous tumors were induced by inoculating 4×10^6 B78-D14 cells into the right flank. Once tumors reached 500 mm^3, mice were randomly divided into two groups (n=6 per group). One group of animals received an intravenous injection of 150 µg (7.5 mg/kg) of Sulfo-Cy5-NHS-labeled ch14.18, and the other group received 150 µg of Sulfo-Cy5-NHS-labeled ch14.18-MMAE. Half of the animals from each group were euthanized after 24 hours, and the other half after 48 hours, followed by processing of tissue samples as described earlier.[20]

In vivo antitumor efficacy

Antitumor efficacy of anti-GD2 ADCs was analyzed in the B78-D14 and EL-4 syngeneic cancer models. For analysis in the B78-D14 model, mice were randomly divided into four groups (n=4 per group) when tumors reached 50 mm^3 volume. Three groups received intravenous injections of 100 µg (5 mg/kg) ch14.18-MMAE, ch14.18-MMAF, or naked antibody for five times with an interval of 4 days, and the control group was injected with PBS. All animals were euthanized when the average tumor volume in the control group reached 1000 mm^3. The EL-4 model was obtained as described before.[15] When the subcutaneous tumors reached 100–200 mm^3, mice were divided into three groups. Two groups received intravenous injections of 100 µg (5 mg/kg) ch14.18-MMAF or naked antibody for five times with an interval of 3 days, and the control group was injected with PBS. All animals were euthanized when the average tumor volume in the control group reached 2500 mm^3. Tumor volumes were measured by the modified ellipsoidal formula V = (length × $width^2$)/2 two times weekly. Both cancer models form

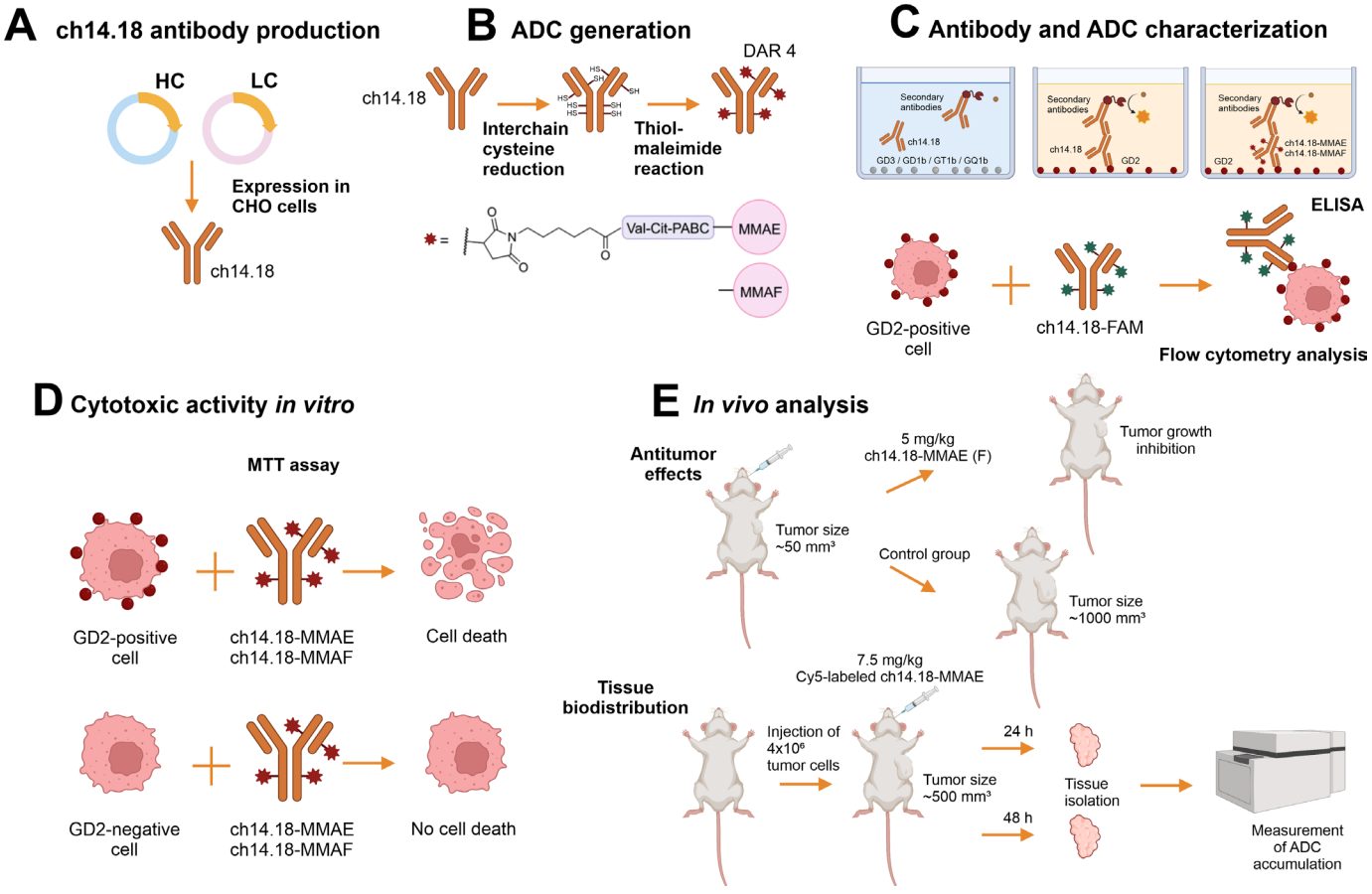

Figure 1 The main experimental stages of the work. The ch14.18 antibody was produced by stable expression in CHO cells (A), and its conjugation with the small molecules MMAE or MMAF was performed by thiol-maleimide chemistry (B). Specific binding of the parent antibody to ganglioside GD2 and preservation of the antigen-binding properties for the ADCs were analyzed by ELISA and flow cytometry (C). The cytotoxic effects of ch14.18-MMAE and ch14.18-MMAF were evaluated in vitro in a panel of tumor cell lines of neuroblastoma, glioma, sarcoma, melanoma, and breast cancer (D), while their antitumor effects and biodistribution in vivo were studied in the B78-D14 melanoma and EL-4 lymphoma mouse models (E). The illustrations were created using BioRender (BioRender.com). ADC, antibody-drug conjugate; DAR, drug-to-antibody ratio; MMAE or MMAF, monomethyl auristatin E or F.

encapsulated tumor masses that do not spontaneously metastasize.

Statistical analysis

Graphs were created using SigmaPlot and GraphPad Prism software. Data are represented as mean±SEM of at least three independent experiments or one representative experiment from three. Statistical analysis was performed using unpaired Student's t-test. Significance levels of $p<0.05$ were considered statistically reliable.

The main stages of the experimental work are graphically presented in figure 1.

RESULTS

Production of ch14.18 antibody

We designed the chimeric GD2-specific antibody 14.18 based on the sequence of variable antibody domains reported by Bolesta *et al*[21] that were ligated with constant domains of the human IgG1κ isotype (see online supplemental file 1). Following stable expression in Chinese hamster ovary (CHO) DG44 cells and purification by protein G chromatography, the resultant product was analyzed by size-exclusion chromatography (online supplemental figure S1E) and SDS-PAGE; the bands on the gel on figure 2A correspond to the heavy and light antibody chains.

We also carried out direct ELISA in order to verify specificity of the ch14.18 antibody for GD2 in the absence of cross-reactivity to other gangliosides. The 14G2a antibody was taken as a positive GD2-specific control since both molecules belong to the same antibody family 14.18/14G2a.[22] Ch14.18 effectively bound GD2, and its binding was comparable to 14G2a (figure 2B). Similar antigen binding of the two antibodies was also observed using confocal microscopy. To this end, GD2-positive EL-4 mouse lymphoma cells were stained by ch14.18-FAM and 14G2a-AF488 (online supplemental figure S1A–D). Furthermore, we demonstrated the absence of cross-reactivity of ch14.18 to other b-series gangliosides GD3, GD1b, GT1b, and GQ1b that are structurally similar to

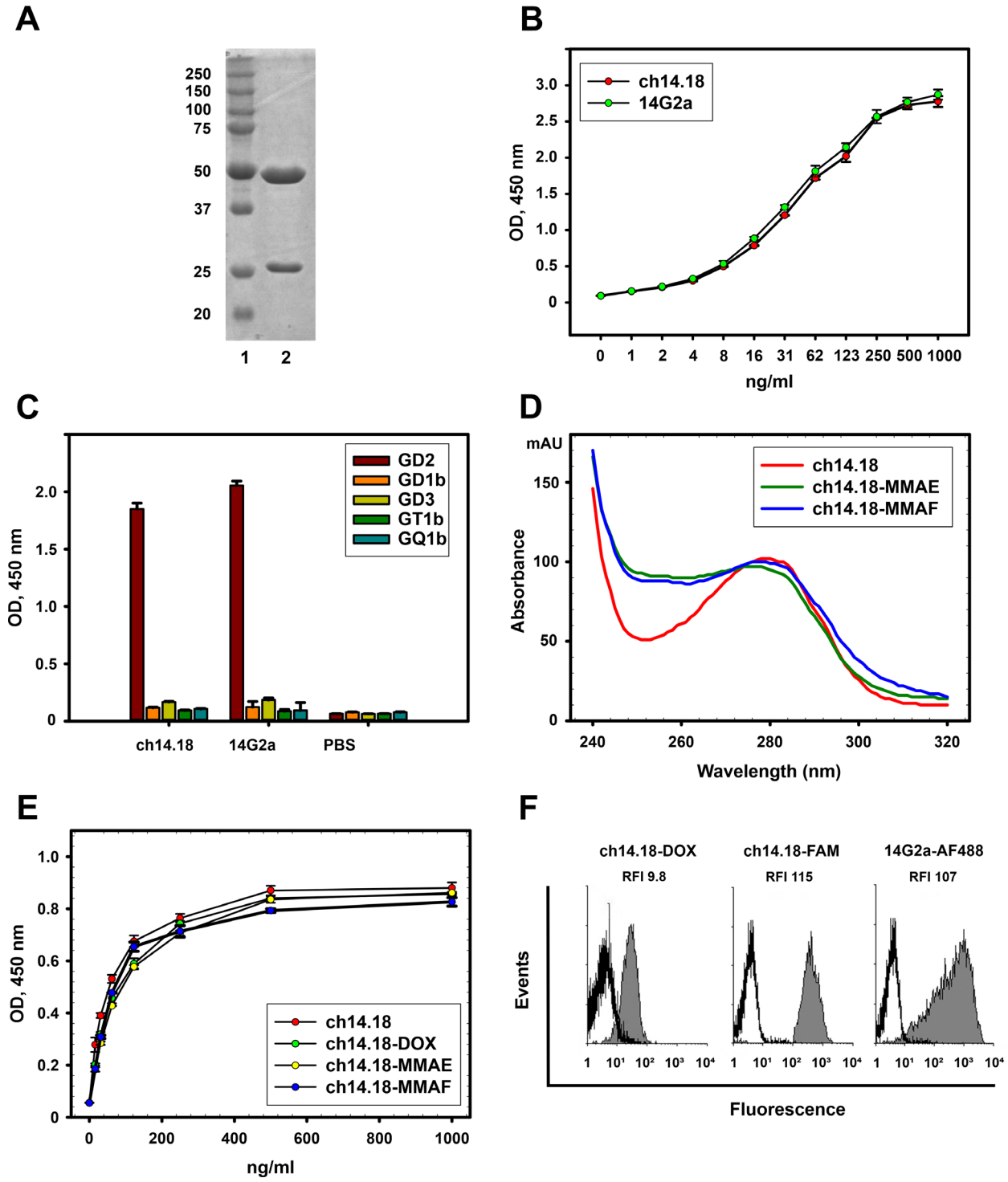

Figure 2 Characterization of the ch14.18 antibody and anti-GD2 ADCs. (A) Reducing polyacrylamide gel electrophoresis of ch14.18 antibody; 1, molecular weight protein markers (Thermo Fisher Scientific); 2, ch14.18. (B) Antigen-binding properties of ch14.18 and 14G2a antibodies analyzed by ELISA; GD2 was adsorbed on the plate. (C) Cross-reactivity of ch14.18 and 14G2a antibodies to structurally similar gangliosides in direct ELISA. GD2, GD3, GD1b, GT1b, or GQ1b were adsorbed on the plate. Ch14.18 or 14G2a antibodies were added in 10 µg/mL concentration; (D) UV-VIS spectra of the ADCs and the parent ch14.18 antibody normalized at 280 nm. (E) Antigen-binding properties of the ADCs analyzed by ELISA; GD2 was adsorbed on the plate. (F) Flow cytometry analysis of EL-4 cells stained with ch14.18-DOX, ch14.18-FAM, and control 14G2a-AF488. Gray histograms represent staining with the corresponding conjugate and empty histograms represent autofluorescence of unstained cells. Relative fluorescence intensity (RFI) ratios of specific fluorescence of cells stained with fluorescently labeled antibodies to autofluorescence of control unstained cells are shown. While RFI values for cells stained with ch14.18-FAM and 14G2a-AF488 are practically equal (RFI 115 vs 107, respectively), a lower RFI for cells stained with ch14.18-DOX (RFI 9.8) is caused by poorer spectral characteristics of doxorubicin. ADC, antibody-drug conjugate; MMAE or MMAF, monomethyl auristatin E or F; UV-VIS, ultraviolet-visible.

GD2 both at low (0.1 µg/mL) (online supplemental figure S1F) and at high (10 µg/mL) (figure 2C) concentrations; we also observed no cross-reactivity with a-series gangliosides (online supplemental figure S1G).

Generation and characterization of ch14.18-MMAE and ch14.18-MMAF

The GD2-specific ADCs were generated by conjugating microtubule inhibitors MMAE or MMAF to the reduced interchain cysteines of the GD2-specific antibody ch14.18 by a maleimide-containing linker. The resulting ADCs with DAR varying from approximately 2 to 6 as determined by UV-VIS spectroscopy demonstrated high long-term stability at 4°C, and had slightly increased light and heavy chain molecular weight relative to the initial antibody when resolved by gel electrophoresis (online supplemental figure S2), which indirectly indicates conjugation of low molecular weight molecules to the antibody. We chose a reference DAR of 4 for our study as a typical DAR within clinically approved ADCs. The average DAR for conjugates generated in the optimized reaction conditions comprised 4.4±0.3 for ch14.18-MMAE and 4.1±0.2 for ch14.18-MMAF in between batches of conjugates (n=5, presented as mean±SEM). Figure 2D depicts absorbance spectra of the ch14.18 antibody and ch14.18-based ADCs normalized at 280 nm; it can be seen that relative absorbance at approximately 250 nm between major peaks increases for the ADCs compared with the parent antibody.

To confirm the average number of drugs conjugated per antibody molecule, ch14.18 conjugates with FAM-maleimide or aldoxorubicin were generated in identical reaction conditions; the average DOL for the fluorescently labeled conjugates roughly corresponded to the molar ratios obtained for the aforementioned ADCs and constituted 4.1 fluorophore molecules per antibody for ch14.18-FAM and 4.6 for ch14.18-DOX.

All generated conjugates demonstrated high binding to GD2 in direct ELISA that was not statistically different from the parent antibody (figure 2E), indicating that conjugation with the drugs by the method used does not affect antigen-binding properties of the antibody. These results were further confirmed by flow cytometry analysis of EL-4 cells stained with ch14.18-FAM or ch14.18-DOX, as well as with the control GD2-specific antibody 14G2a-AF488 (figure 2F), all three of which efficiently stained the cells.

Cytotoxic effects of anti-GD2 ADCs *in vitro*

Since the efficacy of GD2-targeted therapy may correlate with the expression level of GD2 on the surface of tumor cells,[7] cell lines were differentiated by expression of GD2 using flow cytometry prior to the cytotoxicity analysis. We have selected cell lines in such a way that for each type of GD2-positive tumor, cell lines with different level of GD2 expression were present. Five groups of human tumor cell lines were selected: neuroblastomas IMR-32, SH-SY5Y, and NGP-127; gliomas T98G, 1321N1, and U87MG; osteosarcomas U2OS, MG-63, and HOS; breast cancers Hs578T, MCF-7, and SKBr3; melanomas COLO-38, mS, and A375. Additionally, we have analyzed several murine tumor cell lines with different levels of GD2 expression, namely EL-4 lymphoma and B78-D14, B16, and M3 melanomas. This cell line panel was analyzed for GD2 expression using the FAM-labeled ch14.18 antibody, which exhibits similar characteristics to the reference 14G2a antibody (figure 1F) that was used to analyze GD2 expression in our previous works.[18] Thus, selected cell lines were categorized according to relative fluorescence intensity (RFI) values as overexpressing ($GD2^{++++}$; RFI >25), high ($GD2^{+++}$; 10<RFI<25), medium ($GD2^{++}$; 5<RFI<10), low ($GD2^{+}$; 2<RFI<5), or negative ($GD2^{-}$; RFI <2). Results of the study are shown in figure 3A,B and online supplemental figure S3 and are summarized in online supplemental table S2.

A strong dependency of cytotoxic effects of both ch14.18-MMAE and ch14.18-MMAF on the expression of GD2 was observed in murine cell lines (figure 3C,D). Both ADCs effectively inhibited viability of murine EL-4 lymphoma and B78-D14 melanoma expressing the highest GD2 level among all murine and human cell lines within the study (RFI 59±8 and 98±4, respectively). The initially selected nanomolar concentration interval did not allow to determine IC50 values for ch14.18-MMAE and ch14.18-MMAF in EL-4 and B78-D14 cells (figure 3C,D), so they were calculated by decreasing ADC concentration to the picomolar range and constituted 292±85 pM and 62±9 pM for EL-4 lymphoma and 442±170 pM and 48±9 pM for B78-D14 melanoma, respectively (online supplemental figure S4). Simultaneously, cytotoxic effects were not observed in GD2-negative B16 and M3 melanomas even for high concentrations of the ADCs. Notably, the B78-D14 cell line is an amelanotic variant of the B16 line that was modified to express GM2/GD2 and GD3 synthases,[17] meaning that the two lines are almost identical genetically and primarily differ in GD2 expression, thereby representing an adequate pair for the comparison of efficiency of anti-GD2 ADCs.

Both free MMAE and MMAF inhibited growth of all murine cell lines in the study, yet MMAE had a significantly stronger cytotoxic effect compared with MMAF in all cases (figure 3E,F; $p<0.05$). IC50 for both drugs in murine tumor cell types varied to some extent but there was no correlation between expression level of GD2 and cytotoxicity, implying that selectivity is achieved only when the drugs are conjugated to GD2-specific antibodies.

In our earlier works, we showed that murine GD2-specific antibodies 14G2a induced direct cell death in GD2-positive tumor lines.[8 23] In this regard, it seemed important to assess the direct contribution of ch14.18 antibodies to the cytotoxic effects exhibited by the ADCs in the selected murine lines. Data for both 14G2a and ch14.18 are shown in figure 3G,H. In contrast to 14G2a that induced strong selective effects in GD2-positive cells, ch14.18 demonstrated only weak effects in a wide range of concentrations. These results show that the induction

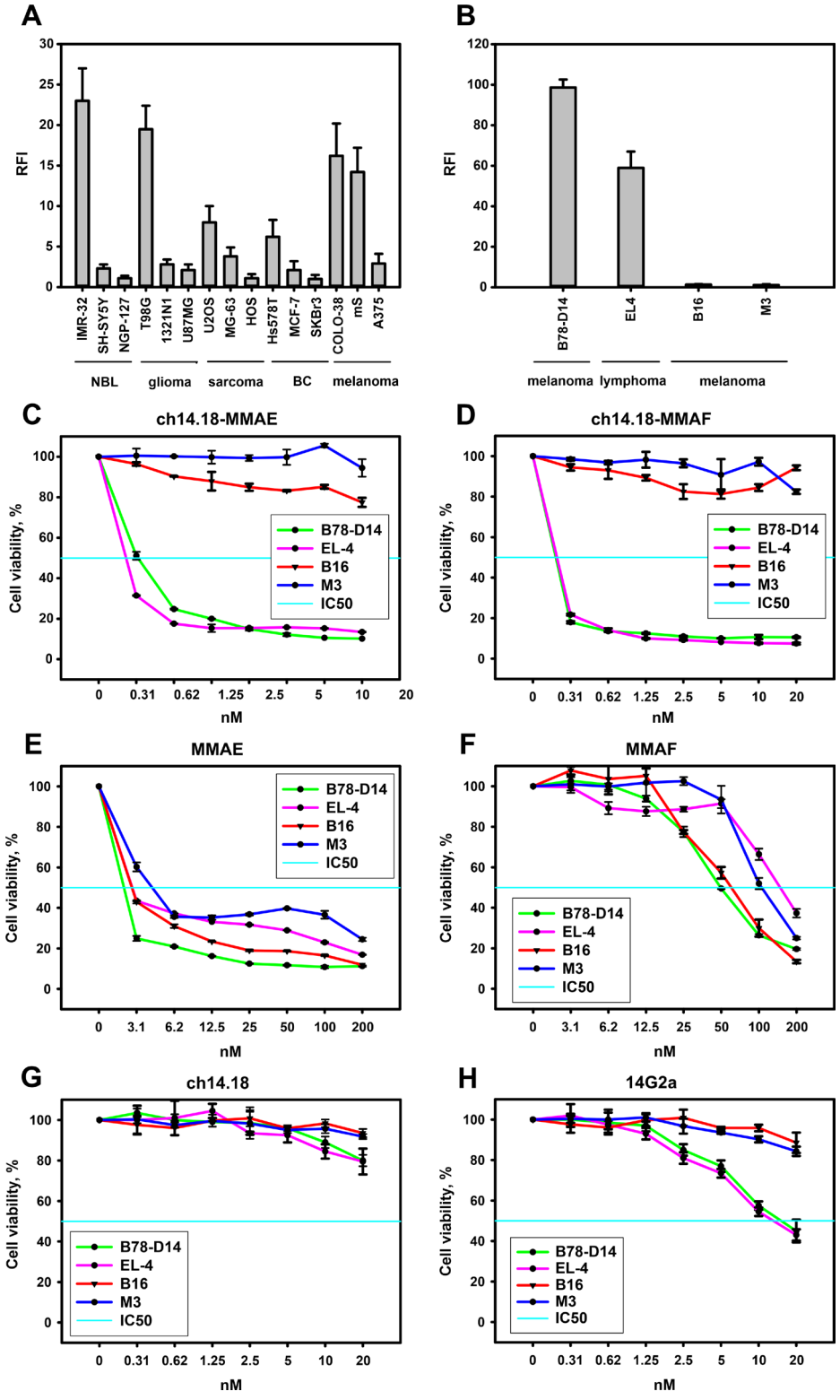

Figure 3 GD2 expression level and cytotoxic activity of anti-GD2 ADCs in murine cell lines. (A,B) Flow cytometry analysis of ganglioside GD2 expression performed with ch14.18-FAM in a panel of human (A) and murine (B) tumor cell lines. For human neuroblastoma, osteosarcoma, and breast cancer (BC), cell lines with high (IMR-32, U2OS, and Hs578T—one per tumor type, respectively), low (SH-SY5Y, MG-63, and MCF-7) GD2 expression, or complete absence of GD2 expression (NGP-127, HOS, and SKBr3) were analyzed. All human glioma and melanoma cell lines expressed GD2 to some extent, but the level of expression varied significantly. Murine EL-4 lymphoma and B78-D14 melanoma exhibited GD2 overexpression, while the two other murine melanomas M3 and B16 were characterized by the absence of GD2 expression. (C–H) Viability of murine cell lines with varying expression of ganglioside GD2 analyzed by MTT assay following 72 hours incubation with ch14.18-MMAE (C), ch14.18-MMAF (D), MMAE (E), MMAF (F), ch14.18 antibody (G), or 14G2a antibody (H). ADC, antibody-drug conjugate; MMAE or MMAF, monomethyl auristatin E or F; NBL, neuroblastoma; RFI, relative fluorescence intensity.

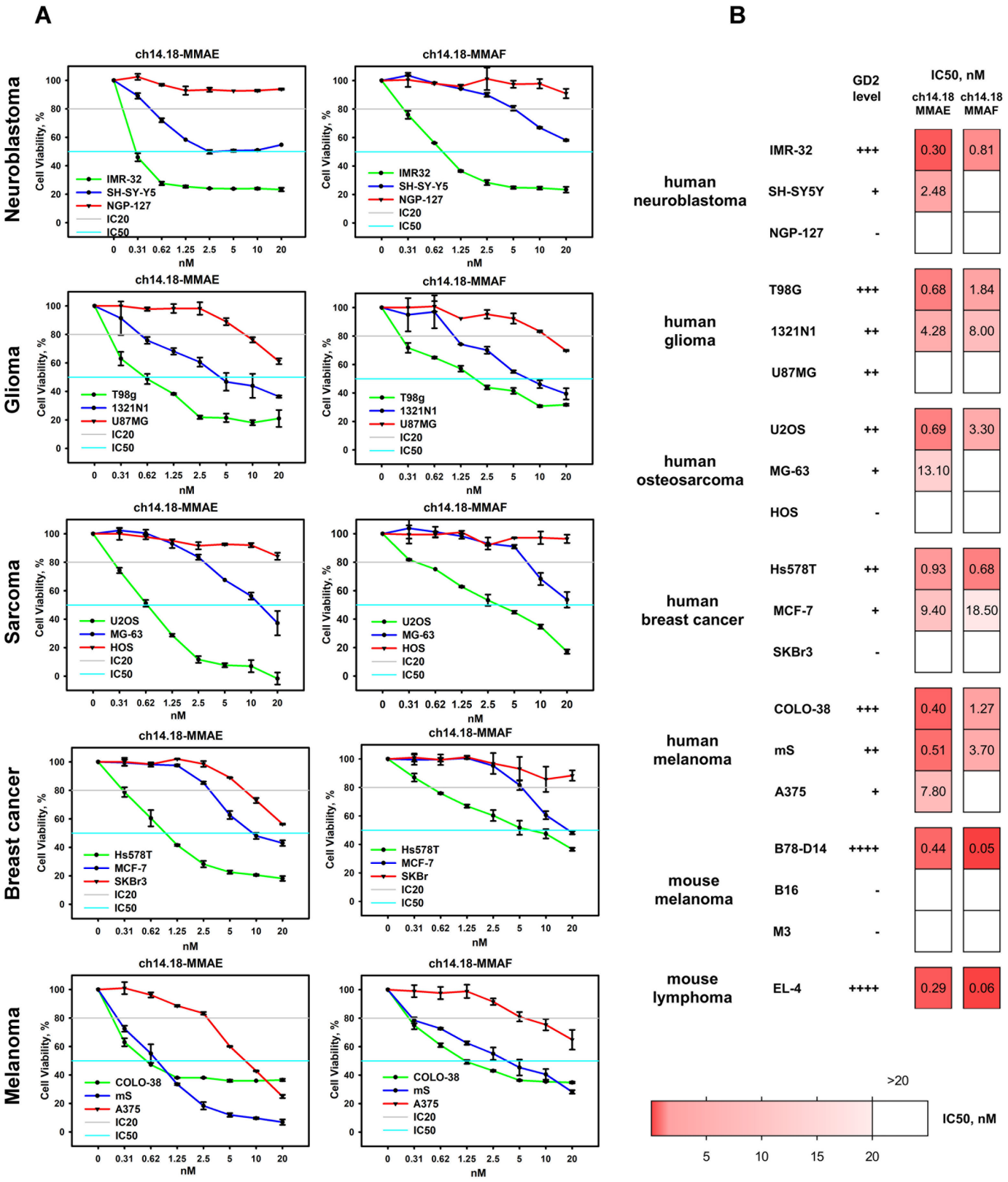

Figure 4 Cytotoxic activity of anti-GD2 ADCs in human cell lines. (A) Viability of human cell lines with varying expression of ganglioside GD2 analyzed by MTT assay following 72 hours incubation with ch14.18-MMAE (left) or ch14.18-MMAF (right). (B) Correlation heatmap between ganglioside GD2 expression and IC50 values of ch14.18-MMAE and ch14.18-MMAF in the tumor cell line panel. ADC, antibody-drug conjugate; MMAE or MMAF, monomethyl auristatin E or F.

of cell death by GD2-specific ch14.18-MMAE and ch14.18-MMAF is mostly due to the small molecule drug activity.

Similarly to the effects in murine cell lines, the cytotoxic effects of the two ADCs in human cell lines strongly correlated with GD2 expression (figures 3A and 4, online supplemental table S2). Ch14.18-MMAE showed significant effects in IMR-32, T98G, U2OS, Hs578T, COLO-38, and mS cell lines with high (10<RFI<25) and medium (5<RFI<10) GD2 expression, with IC50 below 1 nM. Simultaneously, the effects of ch14.18-MMAE were weaker in the cells with low GD2 expression, namely SH-SY5Y, U87MG, and MCF-7, although still evident (figure 4). Finally, its effects in GD2-negative NGP-127, HOS, and SKBr3 were minimal in the selected concentration range and did not reach IC20 (figure 4A). Ch14.18-MMAF was less potent in human cells compared with ch14.18-MMAE, with IC50 values less than 2 nM only in IMR-32, T98G, and COLO-38 cells characterized by high GD2 expression. At the same time, a direct correlation between cytotoxic response and GD2 expression was also observed for this conjugate, with no response in GD2-negative cells in the selected range of concentrations (figure 4 and online supplemental table S2).

It is noteworthy that ch14.18-MMAE demonstrated slightly lower yet similar IC50 values in human IMR-32, T98G, COLO-38, and mS cells with high GD2 expression compared with murine EL-4 and B78-B14 cells overexpressing GD2. At the same time, ch14.18-MMAF was significantly more potent in murine cells with GD2 overexpression than in human cells with high GD2 expression (figures 3 and 4, online supplemental table S2).

Biodistribution of anti-GD2 ADCs in the B78-D14 syngeneic cancer model

The B78-D14 cell line was used to create the mouse cancer model since it forms solid tumors (online supplemental figure S5A) that resemble human melanomas, allowing to adequately analyze the effects of GD2-targeted drugs. The ch14.18-MMAE was chosen for the analysis of accumulation in the tumor and tissue distribution. Fluorescently labeled ch14.18-MMAE variants with DAR 2.8±0.2 and 4.4±0.3 were characterized by contrasting stability, and while ch14.18-MMAE DAR 4.4 started degrading already after conjugation resulting in low binding to GD2 in direct ELISA, ch14.18-MMAE DAR 2.8 showed antigen-binding comparable to that of the labeled parent antibody (online supplemental figure S6).

C57BL/6 mice bearing subcutaneous B78-D14 melanoma tumors were injected with labeled ch14.18-MMAE (DAR 2.8) or the control antibody, and biodistribution in blood plasma and major organs was analyzed 24 hours and 48 hours after injection. Data presented as percentage of the injected dose per gram of the corresponding tissue are summarized in figure 5A and online supplemental table S3. Accumulation of ch14.18-MMAE in the tumor was similar to the control antibody at both time points, demonstrating an increase from 3.6±0.8% vs 3.9±0.5% (ID/g) at 24 hours to 7.7±0.8% vs 6.4±1.1% at 48 hours for ch14.18-MMAE and the control antibody, respectively. Overall, the two molecules showed a comparable biodistribution profile, which is consistent with previous reports on ADCs with low DAR (typically less than 6) evaluated together with corresponding unconjugated antibodies.[24] As was expected, a high quantity of both injected molecules accumulated in the liver at both time points compared with the other analyzed organs.

Antitumor effects of anti-GD2 ADCs

Both ADCs effectively inhibited tumor growth when intravenously injected into mice bearing subcutaneous B78-D14 melanoma tumors, which was clearly seen at all stages of the study (figure 5B). At the end of the experiment, when tumors in the control group reached approximately 1000 mm^3, the average tumor size in the groups treated with ch14.18-MMAE and ch14.18-MMAF was 2.6 times and 3.8 times smaller, respectively, which was significantly smaller (n=4, p<0.05) compared with the control. Although a tendency for higher activity of ch14.18-MMAF relative to ch14.18-MMAE was observed (figure 5B, online supplemental figure S5), the difference was not statistically significant. Also, while the immunocompetent mouse model used in the study enabled the manifestation of all mechanisms of activity for the full-length ch14.18 antibody, no significant difference was observed between tumor growth in the control group and the group injected with ch14.18.

Similar results were obtained in the EL-4 lymphoma mouse model. Despite the tumor growth in this model being much more aggressive compared with the B78-D14 model, ch14.18-MMAF demonstrated a significantly stronger antitumor effect (n=4, p<0.05) compared with the control group, with the tumor size in the group treated with ch14.18-MMAF being on average 2.5 times smaller compared with the control (figure 5C).

DISCUSSION

Despite significant progress in the development of GD2-directed immunotherapies and strong potential of ADCs realized in more than 10 approved drugs, no studies have addressed anti-GD2 ADCs in recent years. However, multiple studies are underway exploring ADCs targeting alternative markers in GD2-expressing tumors.[1] In neuroblastoma, an ADC targeting the neural cell adhesion molecule (CD56) has recently been evaluated in the clinical setting (NCT02452554), while B7-H3,[25] anaplastic lymphoma kinase, galectin-3 binding protein, and glypican 2[26] have all been proven to be effective targets for ADCs in preclinical models. Active clinical trials explore ADCs directed to the AXL receptor tyrosine kinase in breast cancers, melanoma, and sarcomas (NCT03425279; NCT02988817), and to the B7-H3 molecule in TNBC and melanoma (NCT03729596). Prospective melanoma markers already evaluated as ADC targets in the clinic also include the receptor tyrosine kinases ROR2 (NCT03504488) and c-KIT (NCT02221505).[27]

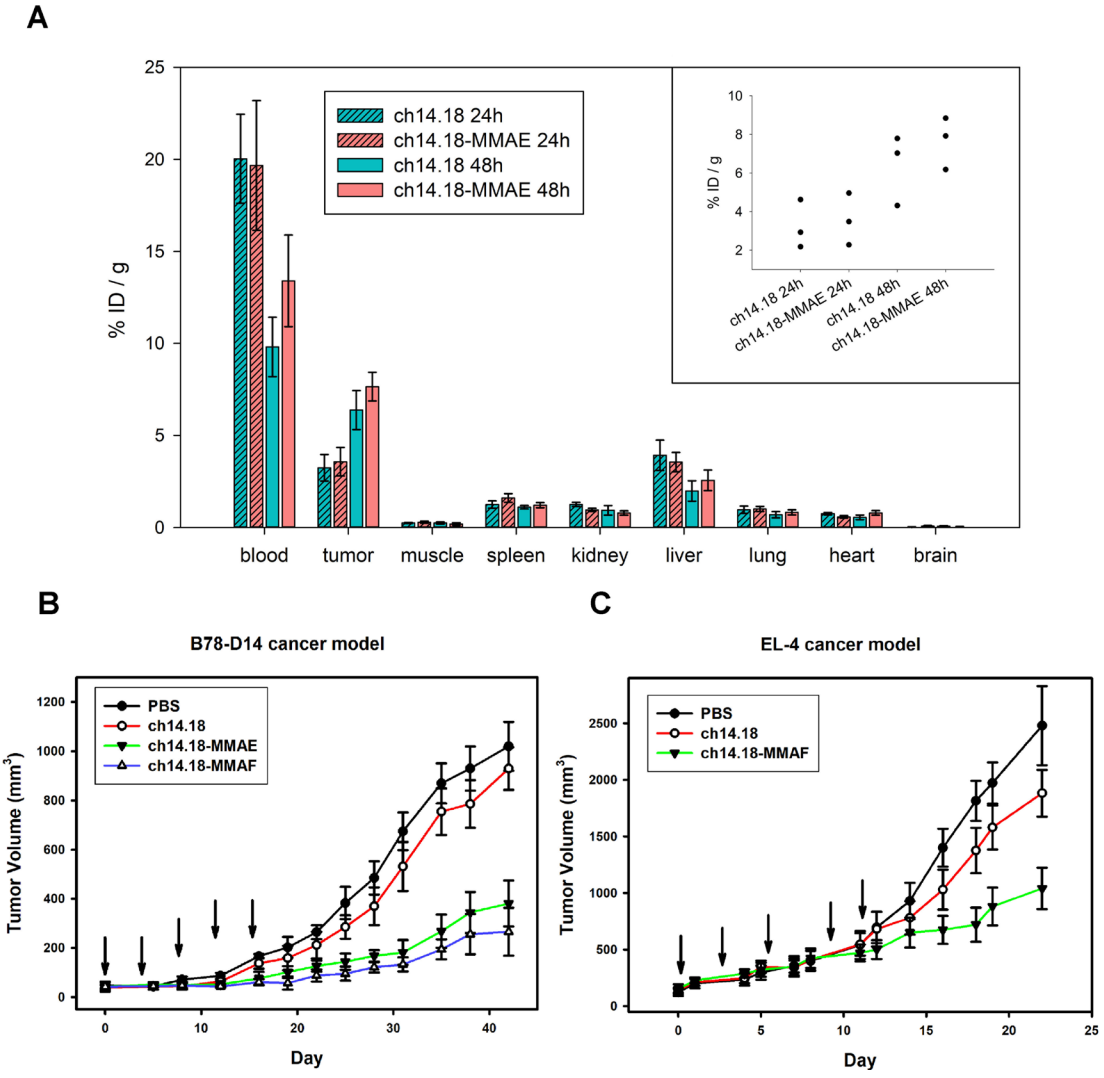

Figure 5 Tissue biodistribution and antitumor efficacy of anti-GD2 ADCs in vivo. (A) Tissue biodistribution following intravenous administration of fluorescently labeled ch14.18-MMAE (DAR 2.8) or its parent antibody ch14.18 in B78-D14 melanoma-bearing C57BL/6 mice at 24 hours and 48 hours post-injection. Data are presented as percentage of injected dose per gram of tissue type (% ID/g), and values represent the mean±SEM derived from groups of three animals. Additionally, for accumulation in the tumor, individual data points for both molecules are presented in a dot plot. In order to measure biodistribution in tissues with minimal blood contamination, residual blood was removed by transcardial perfusion with heparinized PBS following euthanasia. (B), Antitumor activity of ch14.18-MMAE, ch14.18-MMAF, and the parent antibody ch14.18 (each at 5 mg/kg body weight) in B78-D14 melanoma-bearing C57BL/6 mice. When the tumors in the control group reached approximately 1000 mm^3, the tumor size in experimental groups constituted 266±97 mm^3 for mice treated with ch14.18-MMAF, 381±93 mm^3 for mice treated with ch14.18-MMAE, and 930±87 mm^3 for those treated with the parent antibody; values represent the mean±SEM derived from groups of four animals. (C,) Antitumor activity of ch14.18-MMAF and the parent antibody ch14.18 (5 mg/kg) in EL-4 lymphoma-bearing C57BL/6 mice. Values represent the mean±SEM derived from groups of four animals. Arrows indicate the days of ADC administration. Error bars, SEM. ADC, antibody-drug conjugate; DAR, drug-to-antibody ratio; MMAE or MMAF, monomethyl auristatin E or F; PBS, phosphate-buffered saline.

In our work, encouraged by the therapeutic efficacy of ADCs targeting alternative markers in tumors known to overexpress ganglioside GD2, we developed conjugates consisting of the ch14.18 antibody—the most prevalent GD2-specific therapeutic in the clinic, a commonly used cleavable linker, and the auristatins MMAE and MMAF that together are employed in almost half of the currently approved drug conjugates. Their cytotoxic activity was evaluated in tumor cell lines of different origin and with different level of GD2 expression, and in two mouse cancer models.

No data exist in the literature on the effects of anti-GD2 ADCs in human tumor cells expressing GD2, therefore, we performed an analysis of the activity of ch14.18-MMAE and ch14.18-MMAF in a wide panel of cell lines with varying expression of GD2. The first question we set to analyze by in vitro experiments regarded effects of the ADCs in cell lines of different origin. Ganglioside GD2

is a recognized marker in neuroblastoma, and is actively studied as a potential target in gliomas, melanomas, and sarcomas.[8] Additionally, it has recently been shown that GD2 can serve as a marker of breast cancer.[28] In light of the clinical success of ADCs in breast cancer and a limited number of available markers, specifically in TNBC, it seemed important to assess the activity of the conjugates in breast cancer cell lines. We show that regardless of the type of cancer, anti-GD2 ADCs are able to induce the death of tumor cells expressing GD2, which suggests the potential of ADC applicability for the entire wide spectrum of GD2-positive tumors.

The second question addressed by in vitro experiments was the dependence of cell line response to ADCs on the level of surface expression of GD2. The efficiency of targeted therapy can often be hindered by low expression of the tumor antigen.[1] Specifically, while GD2 expression during tumor transformation increases by several orders of magnitude and reaches 10^7 molecules per cell,[29] some studies have shown that its levels in tumors may strongly vary.[7 30] Therefore, cell lines with different GD2 expression were selected for each analyzed cancer type. We demonstrated the activity of both ch14.18-MMAE and ch14.18-MMAF in all GD2-positive cell lines and observed no activity in GD2-negative ones. ADCs demonstrated maximal cytotoxicity (picomolar IC50 values) in the cell lines overexpressing GD2, and it decreased with a decrease in GD2 expression. The conjugates used for the in vitro experiments had DAR=4 common for ADCs,[31] however it is possible to optimize anti-GD2 ADCs to target cells with low antigen expression by increasing DAR and thus achieving a stronger cytotoxic response, an approach that was successfully implemented with anti-HER2 ADC trastuzumab deruxtecan.[32] Overall, we observed a direct dependence of the cytotoxic effect on the level of GD2 expression. IC50 were different for some cell lines characterized by comparable RFI values, which could be explained by different internalization rates of the ADC/GD2 complex. An important parameter, internalization of anti-GD2 ADCs requires additional studies. Nevertheless, high cytotoxicity of our ADCs in GD2-positive cell lines indirectly indicates a significant internalization of the complex. While active internalization is considered to be an immune escape mechanism for naked GD2-specific antibodies,[33] the same process enhances efficiency of drug conjugates in eliminating tumor cells.

An important objective of the in vitro analysis was to compare antitumor activity of the MMAE-conjugated and MMAF-conjugated ADCs in GD2-expressing cell lines. MMAE and MMAF are an example of structurally similar molecules that manifest key differences in intracellular processing and often contrasting efficacy.[1 34] MMAE is membrane-permeable and can therefore not only enter target cells on antibody-mediated delivery but also diffuse into neighboring cells, leading to bystander killing.[35] In contrast, MMAF has limited ability to passively enter or exit the cell due to a phenylalanine moiety at its C-terminus, which results in its lower cytotoxic activity, a fact that we confirmed in our cell lines. Also, unlike MMAE, MMAF is a poor substrate for the multidrug resistance protein 1 efflux pump that tumor cells overexpress as a resistance mechanism to therapy.[34] In our experiments, ch14.18-MMAF was more effective than ch14.18-MMAE in murine cell lines overexpressing GD2, while ch14.18-MMAE had a more prominent activity in cell lines expressing low levels of GD2, and these differences are likely to stem from the properties of the small molecules. Since high antigen density on the cell surface leads to a stronger internalization of the ADCs and drug accumulation inside the cell, it may be speculated that MMAF-conjugated antibodies would be more effective for the therapy of tumors with high GD2 expression, whereas the bystander effect of MMAE would help MMAE-conjugated antibodies to more efficiently eradicate tumors expressing low levels of the antigen. In this regard, an approach employing ADCs simultaneously carrying both MMAE and MMAF may be justified, since GD2-expressing tumors are often characterized by a high degree of antigen heterogeneity. Enhanced cytotoxic properties in cell lines and in vivo models were recently demonstrated for such conjugates compared with antibodies conjugated to each drug variant.[34 36]

In our work, for the first time, an analysis of antitumor effects of anti-GD2 ADCs was performed in a solid GD2-positive tumor. The only published work on anti-GD2 ADCs describes a disseminated GD2-positive cancer model.[13] We used the B78-D14 cell line in order to create a syngeneic solid cancer model that was characterized by rapid and reproducible growth in our experiments. Proceeding to in vivo studies, it was important to analyze biodistribution and accumulation of anti-GD2 ADCs in the tumor compared with their parent antibody. Antibodies are characterized by prolonged circulation time in the body and minimal filtration through the kidneys due to their large size and the neonatal Fc receptor-mediated recirculation.[37] Conjugation of the ch14.18 antibody with small molecules did not change the biodistribution profile. At 48 hours postadministration large amounts of both the naked antibody and ch14.18-MMAE were found in the blood, as well as a significant accumulation of both molecules in the tumor. The ADC and its parent antibody showed higher accumulation in the tumor at 48 hours (ID/g ranging from 6.4%–7.7%) compared with 24 hours (3.6%–3.9% ID/g), which falls within the data interval from other biodistribution studies on GD2-specific antibodies performed in alternative mouse models.[38 39]

Since B78-D14 cells were transplanted to immunocompetent mice, the naked chimeric antibody ch14.18 was capable of activating all its corresponding immune mechanisms,[37 40] namely antibody-dependent cell-mediated cytotoxicity and complement-dependent cytotoxicity. In addition, GD2-specific antibodies are able to independently induce direct cell death.[8] However, administration of ch14.18 had an insignificant antitumor effect compared with the control group. A reason for this may be that the murine model B78-D14, a derivative from the

B16 model, is a low immunogenic tumor characterized by downregulation of immune activating genes, high expression of the inhibitory ligand CTLA-4, and low content of infiltrating immune effector cells.[41] In contrast, both ADCs effectively inhibited tumor growth, which was clearly seen at all stages of the study. A first report on effects of anti-GD2 ADCs in a solid tumor model, our data indicate their potential for the therapy of GD2-positive human tumors. At the same time, mice from groups treated with the ADCs did not achieve complete tumor regression.

In vivo efficacy of the developed ADCs was additionally confirmed in a second GD2-positive syngeneic model. The EL-4 mouse lymphoma model is widely used for anticancer drug studies, including those with drugs targeting GD2, due to a high expression of this antigen by EL-4 cells.[42] Despite aggressive tumor growth in this model, strong antitumor activity of the ADCs was confirmed in it, which corresponds to the effects observed in the B78-D14 model. These results together suggest that the antitumor effects of the developed GD2-specific ADCs are of a general nature and can manifest themselves in different in vivo cancer models.

One reason why the GD2-specific ADCs were unable to eradicate tumors in vivo may result from their limited stability in rodent plasma. The classic MC-VC-PABC linker used in our work interacts with antibody cysteines via its maleimide group, while the valine-citrulline dipeptide provides release of the free drug inside the cells through cathepsin-mediated cleavage. The maleimide-thiol bond maintains a degree of stability in circulation but can undergo retro Michael-type addition under physiological conditions,[43] leading to the detachment of the chemotherapeutics from the antibody, which decreases targeted drug delivery and increases systemic toxicity. In a recent study, slow hydrolysis at neutral pH was a likely reason of absence of antitumor response for a maleimide linker-based ADC in a xenograft model of ovarian cancer, although a similar ADC containing the bromoacetamido-linker inhibited tumor growth.[44] Additionally, the presence of valine-citrulline in the linker can add instability to the ADCs in murine blood. Carboxylesterase 1C was shown to be responsible for the extracellular hydrolysis of the VC-PABC-based linker and subsequent release of auristatins into the blood of rodents, but not humans or monkeys.[45]

Incomplete in vivo efficacy of anti-GD2 ADCs in our study could potentially be related to their immunogenicity, since immune responses involving formation of neutralizing antibodies have been reported both for chimeric antibodies and for MMAE and MMAF presented on the antibody molecule as haptens.[46] We did not observe significant levels of neutralizing antibodies in most plasma samples from mice participating in the in vivo efficacy analysis, however neutralizing antibodies with the specificity both to the ch14.18 antibody and to MMAE and MMAF were detected in several animals. On a different note, we observed a decrease of GD2 expression in B78-D14 cells explanted from tumors of mice treated with anti-GD2 ADCs. The increase in the number of cells with low GD2 expression following therapy may indicate a mechanism that limits ADC efficacy. Overall, the findings of the study indicate of the validity of employing ADCs in GD2-expressing tumors and support their further optimization.

Acknowledgements The authors thank David Schrama (University Hospital Wuerzburg, Germany), Jurgen Becker (Universität Duisburg, Germany) and Dmitri Lodygin (University Medical Centre Göttingen, Germany) for their kind help with supply and delivery of the B78-D14 cell line; Dmitry Ryazantsev for assistance with chromatographic purification and Ilya Mikhalyov for providing ganglioside GM2 (both from Shemyakin-Ovchinnikov Institute of Bioorganic Chemistry RAS, Russia); and William Telford (Center for Cancer Research, National Cancer Institute, USA) for providing aldoxorubicin.

Contributors Conception and design: RVK; Development of methodology: RVK, EVS, IVK; Acquisition of data: RVK, DVK, IVK, MVK, AVK, IID, MVG, FNR; Analysis and interpretation of data: RVK, DVK, EVS, SSL, SMD; Writing, review and/or revision of the manuscript: RK, DVK, EVS, IVK, SMD. Administrative, technical or material support: RVK, SMD. Study supervision: RVK. Guarantor: RVK.

Funding The research was supported by the Russian Science Foundation grant 21-74-30016.

Competing interests None declared.

Patient consent for publication Not applicable.

Ethics approval All experiments with mice were approved by the IBCh RAS Institutional Animal Committee, protocol #325, 2021, and performed in compliance with AAALAC guidelines.

Provenance and peer review Not commissioned; externally peer reviewed.

Data availability statement All data relevant to the study are included in the article or uploaded as supplementary information.

ORCID iDs
Daniel V Kalinovsky http://orcid.org/0000-0001-8773-2797
Mariya V Konovalova http://orcid.org/0000-0003-3923-6304
Roman V Kholodenko http://orcid.org/0000-0001-6083-6588

REFERENCES

1 Dean AQ, Luo S, Twomey JD, *et al*. Targeting cancer with antibody-drug conjugates: promises and challenges. *MAbs* 2021;13:1951427.
2 Kaplon H, Reichert JM. Antibodies to watch in 2021. *MAbs* 2021;13:1860476.
3 Baah S, Laws M, Rahman KM. Antibody-drug conjugates-a tutorial review. *Molecules* 2021;26:2943.
4 M. Bordeau B, P. Balthasar J. Strategies to enhance monoclonal antibody uptake and distribution in solid tumors. *Cancer Biol Med* 2021;18:649–64.
5 Zhang X, Leng J, Zhou Y, *et al*. Efficacy and safety of anti-HER2 agents in combination with chemotherapy for metastatic HER2-positive breast cancer patient: a network meta-analysis. *Front Oncol* 2021;11:731210.

6 Burguin A, Diorio C, Durocher F. Breast cancer treatments: updates and new challenges. *J Pers Med* 2021;11:808.
7 Nazha B, Inal C, Owonikoko TK. Disialoganglioside GD2 expression in solid tumors and role as a target for cancer therapy. *Front Oncol* 2020;10:1000.
8 Doronin II, Vishnyakova PA, Kholodenko IV, *et al*. Ganglioside GD2 in reception and transduction of cell death signal in tumor cells. *BMC Cancer* 2014;14:295.
9 Park JA, Cheung N-KV. Targets and antibody formats for immunotherapy of neuroblastoma. *J Clin Oncol* 2020;38:1836–48.
10 Schengrund C-L. Gangliosides and neuroblastomas. *Int J Mol Sci* 2020;21:5313.
11 Shilova O, Shramova E, Proshkina G, *et al*. Natural and designed toxins for precise therapy: modern approaches in experimental oncology. *Int J Mol Sci* 2021;22:4975.
12 Kholodenko IV, Kalinovsky DV, Doronin II, *et al*. Neuroblastoma origin and therapeutic targets for immunotherapy. *J Immunol Res* 2018;2018:1–25.
13 Lode HN, Reisfeld RA, Handgretinger R, *et al*. Targeted therapy with a novel enediyene antibiotic calicheamicin theta(I)1 effectively suppresses growth and dissemination of liver metastases in a syngeneic model of murine neuroblastoma. *Cancer Res* 1998;58:2925–8.
14 Chen Y. Drug-to-antibody ratio (DAR) by UV/VIS spectroscopy. *Methods Mol Biol* 2013;1045:267–73.
15 V Kholodenko I, V Kalinovsky D, V Svirshchevskaya E, *et al*. Multimerization through PEGylation improves pharmacokinetic properties of scFv fragments of GD2-specific antibodies. *Molecules* 2019;24:3835.
16 Molotkovskaya IM, Kholodenko RV, Zelenova NA, *et al*. Gangliosides induce cell apoptosis in the cytotoxic line CTLL-2, but not in the promyelocyte leukemia cell line HL-60. *Membr Cell Biol* 2000;13:811–22.
17 Haraguchi M, Yamashiro S, Yamamoto A, *et al*. Isolation of GD3 synthase gene by expression cloning of GM3 alpha-2,8-sialyltransferase cDNA using anti-GD2 monoclonal antibody. *Proc Natl Acad Sci U S A* 1994;91:10455–9.
18 Sorokin M, Kholodenko I, Kalinovsky D, *et al*. RNA sequencing-based identification of ganglioside GD2-positive cancer phenotype. *Biomedicines* 2020;8:142.
19 Vishnyakova PA, Doronin II, Kholodenko IV, *et al*. Caspases participation in cell death induced by the GD2-specific antibodies. *Russ J Bioorg Chem* 2014;40:279–87.
20 Gracheva I, Konovalova M, Aronov D, *et al*. Size-dependent biodistribution of fluorescent furano-allocolchicinoid-chitosan formulations in mice. *Polymers* 2021;13:2045.
21 Bolesta E, Kowalczyk A, Wierzbicki A, *et al*. DNA vaccine expressing the mimotope of GD2 ganglioside induces protective GD2 cross-reactive antibody responses. *Cancer Res* 2005;65:3410–8.
22 Mujoo K, Kipps TJ, Yang HM, *et al*. Functional properties and effect on growth suppression of human neuroblastoma tumors by isotype switch variants of monoclonal antiganglioside GD2 antibody 14.18. *Cancer Res* 1989;49:2857–61.
23 Doronin II, Kholodenko IV, Zubareva AA, *et al*. Involvement of actin filaments in the cytotoxic effect of GD2-specific antibodies. *Bull Exp Biol Med* 2019;166:541–7.
24 Sun X, Ponte JF, Yoder NC, *et al*. Effects of drug-antibody ratio on pharmacokinetics, biodistribution, efficacy, and tolerability of antibody-maytansinoid conjugates. *Bioconjug Chem* 2017;28:1371–81.
25 Kendsersky NM, Lindsay J, Kolb EA, *et al*. The B7-H3-targeting antibody-drug conjugate m276-SL-PBD is potently effective against pediatric cancer preclinical solid tumor models. *Clin Cancer Res* 2021;27:2938–46.
26 Buongervino S, Lane MV, Garrigan E, *et al*. Antibody-drug conjugate efficacy in neuroblastoma: role of Payload, resistance mechanisms, target density, and antibody internalization. *Mol Cancer Ther* 2021;20:2228–39.
27 Esnault C, Schrama D, Houben R, *et al*. Antibody-drug conjugates as an emerging therapy in Oncodermatology. *Cancers* 2022;14:778.
28 Shao C, Anand V, Andreeff M, *et al*. Ganglioside GD2: a novel therapeutic target in triple-negative breast cancer. *Ann N Y Acad Sci* 2022;1508:35-53.
29 Wu ZL, Schwartz E, Seeger R, *et al*. Expression of GD2 ganglioside by untreated primary human neuroblastomas. *Cancer Res* 1986;46:440–3.
30 Terzic T, Cordeau M, Herblot S, *et al*. Expression of disialoganglioside (GD2) in neuroblastic tumors: a prognostic value for patients treated with anti-GD2 immunotherapy. *Pediatr Dev Pathol* 2018;21:355–62.
31 Hamblett KJ, Senter PD, Chace DF, *et al*. Effects of drug loading on the antitumor activity of a monoclonal antibody drug conjugate. *Clin Cancer Res* 2004;10:7063–70.
32 Ishii T, Shitara K. Trastuzumab deruxtecan and other HER2-targeting agents for the treatment of HER2-positive gastric cancer. *Expert Rev Anticancer Ther* 2021;21:1193–201.
33 Tibbetts R, Yeo KK, Muthugounder S, *et al*. Anti-disialoganglioside antibody internalization by neuroblastoma cells as a mechanism of immunotherapy resistance. *Cancer Immunol Immunother* 2022;71:153–64.
34 Yamazaki CM, Yamaguchi A, Anami Y, *et al*. Antibody-drug conjugates with dual payloads for combating breast tumor heterogeneity and drug resistance. *Nat Commun* 2021;12:3528.
35 Singh AP, Sharma S, Shah DK. Quantitative characterization of in vitro bystander effect of antibody-drug conjugates. *J Pharmacokinet Pharmacodyn* 2016;43:567–82.
36 Levengood MR, Zhang X, Hunter JH, *et al*. Orthogonal cysteine protection enables homogeneous multi-drug antibody–drug conjugates. *Angew Chem Int Ed* 2017;56:733–7.
37 Deyev SM, Lebedenko EN. Modern technologies for creating synthetic antibodies for clinical application. *Acta Naturae* 2009;1:32–50.
38 Vavere AL, Butch ER, Dearling JLJ, *et al*. 64Cu-p-NH2-Bn-DOTA-hu14.18K322A, a PET radiotracer targeting neuroblastoma and melanoma. *J Nucl Med* 2012;53:1772–8.
39 Butch ER, Mead PE, Amador Diaz V, *et al*. Positron emission tomography detects *In Vivo* expression of disialoganglioside GD2 in mouse models of primary and metastatic osteosarcoma. *Cancer Res* 2019;79:3112–24.
40 Overdijk MB, Verploegen S, Ortiz Buijsse A, *et al*. Crosstalk between human IgG isotypes and murine effector cells. *J Immunol* 2012;189:3430–8.
41 Becker JC, Varki N, Gillies SD, *et al*. Long-lived and transferable tumor immunity in mice after targeted interleukin-2 therapy. *J Clin Invest* 1996;98:2801–4.
42 Alvarez-Rueda N, Leprieur S, Clémenceau B, *et al*. Binding activities and antitumor properties of a new mouse/human chimeric antibody specific for GD2 ganglioside antigen. *Clin Cancer Res* 2007;13:5613s–20.
43 Baldwin AD, Kiick KL. Tunable degradation of maleimide-thiol adducts in reducing environments. *Bioconjug Chem* 2011;22:1946–53.
44 Minnix M, Li L, Yazaki P, *et al*. Improved targeting of an anti-TAG-72 antibody drug conjugate for the treatment of ovarian cancer. *Cancer Med* 2020;9:4756–67.
45 Dorywalska M, Dushin R, Moine L, *et al*. Molecular basis of valine-citrulline-PABC linker instability in site-specific ADCs and its mitigation by linker design. *Mol Cancer Ther* 2016;15:958–70.
46 Carrasco-Triguero M, Dere RC, Milojic-Blair M, *et al*. Immunogenicity of antibody-drug conjugates: observations across 8 molecules in 11 clinical trials. *Bioanalysis* 2019;11:1555–68.

Therapeutic efficacy of antibody-drug conjugates targeting GD2-positive tumors

Supplementary Methods

Production of chimeric monoclonal antibody 14.18

The sequences coding for the heavy chain (HC) and light chain (LC) variable domains of the model chimeric antibody were obtained from data reported by Bolesta et al. (2005) and codon-optimized for efficient expression in mammalian cells. The coding sequences of the HC and LC variable domains and secretion signal sequences were then fused to the cDNA of human gamma 1 and kappa constant regions, and cloned into pcDNA3.3-TOPO TA and pOptiVEC-TOPO TA vectors (Invitrogen) using the XhoI/NheI and XbaI/NotI restriction sites, respectively. The chimeric HC and LC expression units were coupled with selection markers.

Parental CHO DG44 (dfhr-/-) cells were cultured in a protein-free medium CD DG44 supplemented with 8 mM GlutaMAX-I and 0.05% Pluronic F-68 (all from Gibco). The plasmid DNA was purified using Qiagen MaxiPrep Kit (Qiagen) and linearized using the unique MluI site. For transfection, $0.5x10^6$ cells, 0.6 µg of plasmid DNA, and 0.5 µg of FreeStyle MAX transfection reagent (Thermo Fisher Scientific) were used per 1 ml of transfection mixture. For batch selection of the stable clones, transfectants were selected in a shaker culture in the medium containing 200 µg/ml of G418 (Sigma-Aldrich) and lacking hypoxanthine/thymidine. Cell pools resistant to the first selection step were subjected to four steps of methotrexate amplification (25-500 nM). Single-cell clones were isolated from the heterogeneously amplified pools by limiting dilution cloning. Selected clones were scaled to shake flasks and cultured in CD OptiCHO medium (Thermo Fisher Scientific) supplemented with 8 mM GlutaMAX-I.

Purification of recombinant proteins was performed on Protein G sepharose (Thermo Fisher Scientific). The prepared culture medium was applied to the column at a rate of 1 ml per minute. Elution was carried out sequentially with three buffer solutions: 0.1 M sodium citrate, pH 3.75; 0.1 M sodium citrate, pH 3.0; and 0.1 M glycine, pH 2.0. The eluates were collected separately, and pH was immediately adjusted to neutral values. Ch14.18 antibodies were then transferred to phosphate buffered saline (PBS) in Amicon Ultra-4 10 kDa centrifugal filters (Merck) and sterilized through a 0.22 µm membrane filter. Protein concentration was calculated at a wavelength of 280 nm by BioDrop µLITE spectrophotometer (BioDrop, UK).

Direct ELISA

Nunc MaxiSorp high protein-binding capacity 96 well ELISA plates (Thermo Fisher Scientific) were coated with gangliosides GD2, GM2, GD1b, and GD3 at concentration of 0.25 µg in 100 µl of 96% ethanol per well. Following air drying, plate wells were blocked with 100 µl 2% BSA in PBS supplemented with 0.1% Tween-20 (PBS-T) per well for 2 h at RT. Chimeric antibody ch14.18 or control mouse antibody 14G2a (Santa Cruz Biotechnology) (100 µl per well in PBS-T) were added in triplicates at different concentrations. Following incubation for 1.5 h and washing with PBS-T, and anti-human or anti-mouse Fc-specific HRP-labeled antibodies (both 1:6000; Santa Cruz Biotechnology) were added to the wells. After 40 min incubation and further washing, 1-Step Ultra TMB-ELISA Substrate Solution (Thermo Fisher Scientific) was added, and the color reaction optical density (OD) was measured at 450 nm by Multiscan FC microplate reader (Thermo Fisher Scientific). Percent of cross-reactivity was calculated as the ratio of TMB color reaction OD_{450} in GM2-, GD1b-, or GD3-coated wells to OD_{450} in GD2-coated wells.

MTT assay

ADC-induced decrease in cell viability was analyzed by colorimetric MTT (Sigma-Aldrich) assay. Tumor cells were cultured in 96 well flat-bottom tissue culture plates (10^4 cells/well, Greiner) with serial dilutions of anti-GD2 ADCs, antibodies (ch14.18 or 14G2a), MMAE, or MMAF for 72 h under standard conditions. Following incubation, the MTT solution (in 250 µg/ml final concentration) was added to each sample for 4 h, and the formazan precipitate was dissolved in DMSO. OD was assessed by Multiscan FC microplate reader at a wavelength of 540 nm. Cell viability was calculated as $(OD_{\text{treated cells}} - OD_{\text{blank}})/(OD_{\text{control cells}} - OD_{\text{blank}}) \times 100\%$, where OD_{blank} represents OD in control wells containing no cells. Dose–response curves were generated using SigmaPlot software. All MTT experiments were reproduced at least three times.

Tissue sample processing for *ex vivo* biodistribution studies.

Blood was collected into heparin treated tubes by retro-orbital bleeds of anaesthetized mice, followed by plasma analysis. Euthanasia was performed with isoflurane. In order to measure biodistribution in tissues with minimal blood contamination, residual blood was removed by transcardial perfusion with 10 ml of heparinized PBS. Tissues were dissected and homogenized, followed by incubation in a hydrochloric acid-ethanol solution overnight at 4 °C. Samples were cleared by centrifugation, and fluorescence intensity was analyzed by GloMax-Multi Detection System fluorometer (Promega) with excitation at 625 nm and absorbance at 660–720 nm. Organs and blood plasma from intact mice were used for subtraction of autofluorescence.

Supplementary Data

Table S1.

Extinction coefficients employed for the calculation of drug-antibody ratio (DAR) by UV-VIS spectroscopy.

Molecule	Extinction coefficients (cm^{-1} M^{-1}) calculated at given wavelength			
	253 nm	**256 nm**	**280 nm**	**494 nm**
ch14.18	84960	93810	205310	26550
MC-VC-PABC-MMAE	21920	-	3220	-
MC-VC-PABC-MMAF	21900	-	2740	-
DOX	-	25180	8620	-
FAM-maleimide	-	-	14770	74380

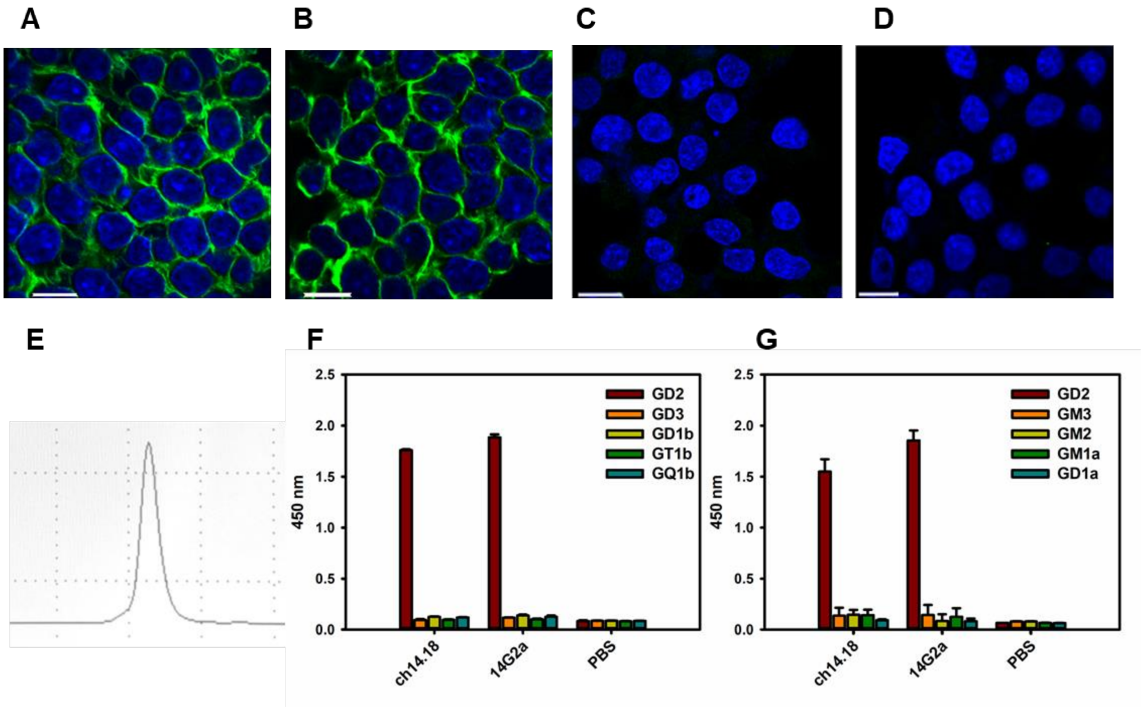

Figure S1.

A-D, Confocal images of GD2-positive mouse lymphoma EL-4 (A, B) and GD2-negative mouse melanoma M3 (C, D) cells stained with antibody conjugates 14G2a-AF488 (A, C) and ch14.18-FAM (B, D). Following staining with fluorescently labeled GD2-specific antibodies and DAPI

(4',6'-diamidine-2-phenylindole, Molecular Probes), cells were fixed and analyzed on the confocal microscope C1 (Nikon, Japan). Staining with anti-GD2 conjugates is shown in green color; the nuclei are counterstained with DAPI (shown in blue). Bar scale: 10 μm.

E, Size-exclusion chromatographic analysis of ch14.18 antibody performed in PBS eluent at 0.75 ml/min flow rate with detection at 280 nm (Superdex 200 10/300 GL column, Cytiva; Beckman System Gold high-performance liquid chromatography system).

F, Evaluation of cross-reactivity of ch14.18 and 14G2a antibodies to b-series gangliosides in direct ELISA. GD2, GD3, GD1b, GT1b, or GQ1b gangliosides were adsorbed on the plate. Ch14.18 or 14G2a antibodies were added in 0.1 μg/ml concentration.

G, Evaluation of cross-reactivity of ch14.18 and 14G2a antibodies to a-series gangliosides in direct ELISA. GD2, GM3, GM2, GM1a, or GD1a gangliosides were adsorbed on the plate. Ch14.18 or 14G2a antibodies were added in 10 μg/ml concentration.

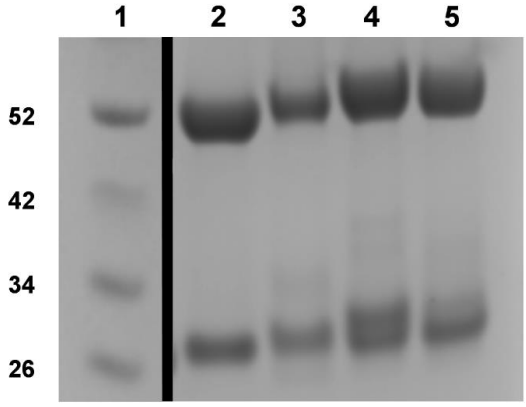

Figure S2.
12% reducing polyacrylamide gel electrophoresis; increased molecular weight of LC and HC observed for the resulting ADCs relative to the initial antibody molecule. 1, molecular weight protein markers; 2, ch14.18 antibody; 3, ch14.18-DOX DAR 4.6; 4, ch14.18-MMAE DAR 4.4; 5, ch14.18-MMAF DAR 4.1.

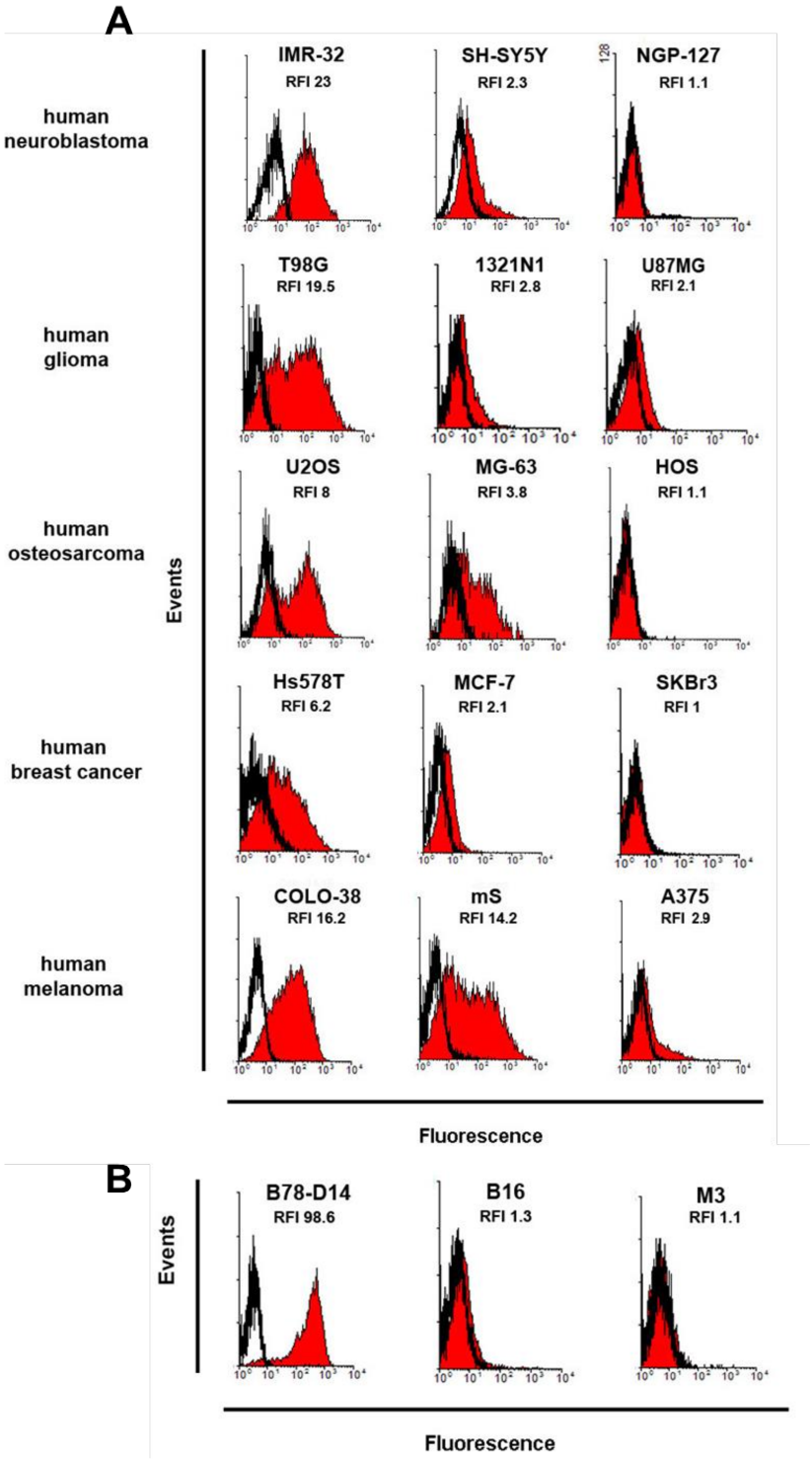

Figure S3.
Flow cytometry analysis of ganglioside GD2 expression in a panel of tumor cell lines. **A**, Staining of human cell lines with ch14.18-FAM. **B**, Staining of murine cell lines with ch14.18-FAM. Red histograms represent staining with ch14.18-FAM, empty histograms represent autofluorescence of unstained cells. RFI – ratio of specific fluorescence of cell staining with fluorescently labeled antibodies ch14.18 and autofluorescence of control unstained cells.

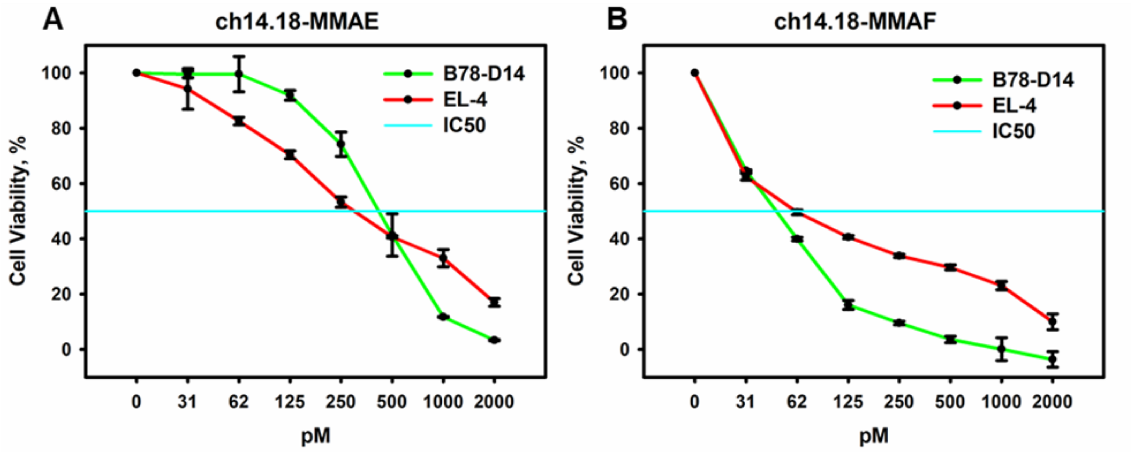

Figure S4.

Viability of murine cell lines with different expression of ganglioside GD2 analyzed by MTT assay following 72 h incubation. **A**, – ch14.18-MMAE, **B**, – ch14.18-MMAF.

Table S2.

Classification of human and murine cell lines by GD2 expression and cell viability following incubation with ch14.18-MMAE and ch14.18-MMAF. RFI calculated by flow cytometry using the ch14.18-FAM conjugate.

Tumor type	Cell lines	Origin	RFI	GD2 level*	IC50%, nM		IC20% nM	
					Ch14.18-MMAE	Ch14.18-MMAF	Ch14.18-MMAE	Ch14.18-MMAF
NBL	IMR-32	H	23±4	+++	0.3±0.1	0.81±0.2	0.15±0.1	0.25±0.1
	SH-SY5Y	H	2.3±0.5	+	2.48±1.2	>40	0.51±0.2	5.3±0.5
	NGP-127	H	1.1±0.3	-	>40	>40	>20	>20
glioma	T98G	H	19.5±3	+++	0.68±0.2	1.84±0.5	0.23±0.1	0.19±0.1
	1321N1	H	2.8±0.6	+	4.28±1.2	8±1.6	0.48±0.2	1±0.3
	U87MG	H	2.1±0.7	+	>40	>40	8.47±2.2	12.4±3.6
sarcoma	U2OS	H	8±2	++	0.685±0.3	3.3±1.5	0.28±0.1	0.3±0.2
	MG-63	H	3,8±1.1	+	13.1±2.8	>20	2.98±1.3	7.3±2.1
	HOS	H	1.1±0.5	-	>40	>40	>20	>20
breast cancer	Hs578T	H	6.2±2.1	++	0.93±0.5	6.8±1.1	0.38±0.2	0.48±0.3
	MCF-7	H	2.1±1.1	+	9.4±1.6	18.5±2.8	3±0.7	5.3±0.8
	SKBr3	H	1±0.5	-	>40	>40	>20	>20
melanoma	COLO-38	H	16.2±4	+++	0.4±0.1	1.27±0.7	0.14±0.1	0.3±0.1
	mS	H	14.2±3	++	0.51±0.2	3.7±0.9	0.2±0.2	0.3±0.1
	A375	H	2.2±1.2	+	7.8±1.4	>40	2.7±0.5	5.3±1.4
	B16	M	1.3±0.3	-	>40	>40	17±2.7	>20
	B78-D14	M	98.6±4	++++	0.442±0.2	0.048±0.01	0.217±0.2	0.024±0.02
	M3	M	1.1±0.4	-	>40	>40	>20	>20
lymphoma	EL-4	M	59±8	++++	0.292±0.1	0.062±0.01	0.086	0.024±0.01

* GD2 level: negative (-), low (+), medium (++), high (+++), overexpression (++++); NBL – neuroblastoma, H – human, M – mouse.

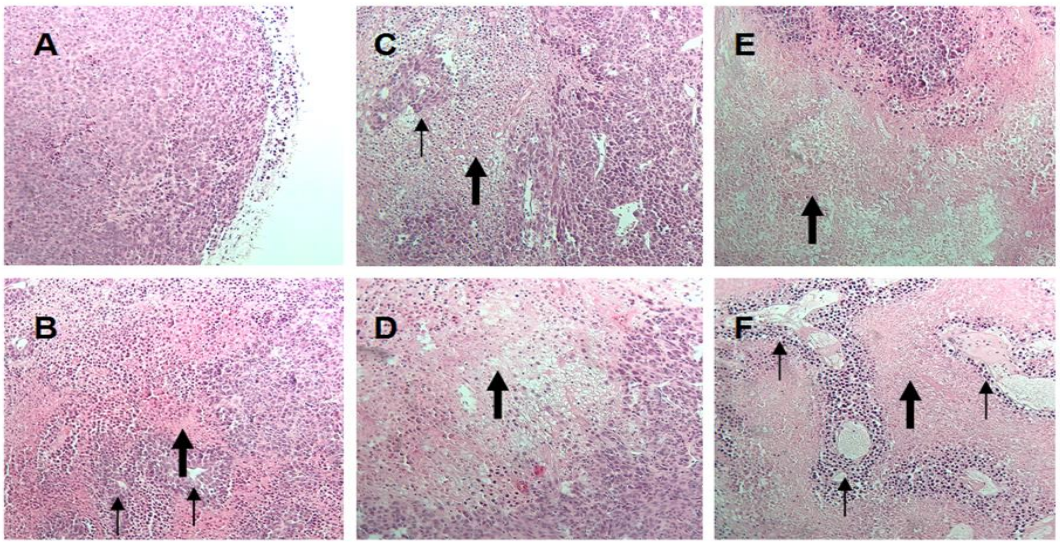

Figure S5.

Histology of control untreated B78-D14 melanoma tumors (**A-B**) and tumors treated with ch14.18-MMAE (**C-D**) or ch14.18-MMAF (**E-F**). Thin arrows indicate blood vessels, thick arrows indicate necrosis zones. Staining with H&E. The B78-D14 melanoma represents a solid tumor (A) with small areas of necrosis (B, thick arrow). Treatment of the tumor with ch14.18-MMAE or ch14.18-MMAF results in the formation of large necrotic zones around blood vessels (C-F). Effect of ch14.18-MMAF is more evident due to larger necrotic zones.

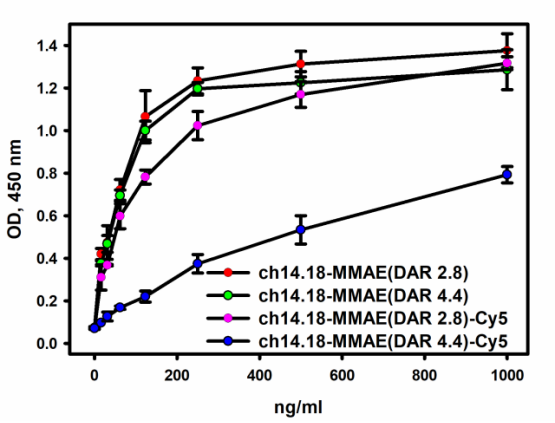

Figure S6.

Analysis of the antigen-binding properties of ch14.18-MMAE and ch14.18-MMAE-Cy5 with DAR 2.8 and DAR 4.4 by direct ELISA; ganglioside GD2 was adsorbed on the plate, serial dilutions of the analytes were added to the wells.

Table S3. Tissue distribution following intravenous administration of ch14.18-MMAE (DAR 2.8) or its parent antibody ch14.18 in C57BL/6 mice at 24 h and 48 h post-injection. Data are presented as % of injected dose per gram of tissue type, and values represent the mean ± S.E.M derived from groups of three animals.

Tissue	ch14.18 24h	ch14.18-MMAE 24h	ch14.18 48h	ch14.18-MMAE 48h
	% ID/g tissue type ± S.E.M.			
Blood	20.03 ± 2.42	19.67 ± 3.53	9.81 ± 1.62	13.40 ± 2.50
Tumor	3.24 ± 0.72	3.57 ± 0.78	6.38 ± 1.06	7.65 ± 0.78
Muscle	0.25 ± 0.02	0.29 ± 0.06	0.24 ± 0.06	0.19 ± 0.07
Spleen	1.25 ± 0.20	1.60 ± 0.24	1.10 ± 0.10	1.21 ± 0.14
Kidney	1.25 ± 0.11	0.96 ± 0.08	0.93 ± 0.26	0.78 ± 0.12
Liver	3.92 ± 0.82	3.55 ± 0.53	1.98 ± 0.55	2.56 ± 0.56
Lung	0.96 ± 0.20	1.01 ± 0.14	0.70 ± 0.17	0.82 ± 0.14
Heart	0.75 ± 0.07	0.57 ± 0.07	0.55 ± 0.13	0.79 ± 0.13
Brain	0.02 ± 0.02	0.08 ± 0.03	0.07 ± 0.02	0.03 ± 0.02